Contactless metal-based EK pump and potential implementations

by

Xiaotong Fu

A thesis submitted to Johns Hopkins University in conformity with the requirements for the degree of Master of Science in Engineering

Baltimore, Maryland

April, 2014

Abstract

Developments of robust microfluidic tools that can manipulate fluids and their contents quickly, easily and without the need for an experienced operator are important requirements in portable diagnostic devices. Among many possible techniques for fluidic pumping and delivering, pressure driven actuation and electrokinetic (EK) flows are the two predominant methods of pumping fluids through small microchannels. Pressure driven devices, however, require large pneumatic support systems and on-chip moving parts that can cause mechanical failure and tedious fabrication process. Electrokinetic pumps do not require moving parts or large off-chip support systems. Traditional EK pumps, however, can suffer from Joule heating, electrode decomposition, and fluid contamination problems due to direct liquid contact with metal electrodes. The bulky volume also makes EK pump integrations become difficult. To overcome these drawbacks, we demonstrate a novel contactless chip-embedded EK pump with polydimethylsiloxane (PDMS) membranes that isolate gallium metal electrodes from the working fluid. Pumping capability was tested and quantified for two different microfluidic channel geometries: a closed circuit “Loop” design and a hydrodynamic resistance free “T-shape” design. Maximum pump pressure and flow rate are 51Pa and 0.3μl/min, respectively, when 2000V is applied. We then utilize these contactless EK pumps by inserting multiple units into a fluid delivery and control system and sample

plug loading system in order to demonstrate their implementations and automation capabilities. This novel contactless gallium pump demonstrates less mechanical failure, lower cost, and higher portability than current EK pumps. This design will facilitate micro-electro-system and lab-on-chip product development and expand their applications in biological study and analytical chemistry.

Acknowledgement

Here I want to take this opportunity to express my gratitude to all the people who helped me in these days. I would like to say thanks to Dr. Zachary Gagnon, who shared his creativity with me in my research He gave me priceless guidance in my lab work and lead my research to a higher level.

I also want to show my appreciation to all of my teammates, Mitch, Nick, Francesca and Markela. Without their help, this research wouldn't be done successfully. Their kindness supported me to go through these days no matter how tough the research was.

I would like to say thanks to my friends, Ning, Zhilin, Qianli and Yumo. Without their encouragement and help, I couldn't adhere to this path and come so far.

At last I really appreciate all the supports from my parents and family. They backed up my life and stay with me no matter what I was facing to. Their loves make up the best part of my life.

Table of Contents

List of Figures

Chapter1 Introduction

1.1 Rising of Lab-on-Chip Product

Microfluidics, also referred as Lab-on-Chip (LOC) products, is an emerging technology that manipulates fluids and performs analysis in micro-channels. These micro-channels usually have a dimension of micron scale. This feature leads to early applications of microfluidic device in biological, chemical analysis as it only requires very small volume of sample and regent. The rising of silicon-based microfluidic device was facilitated by silicon fabrication technology development in 1980s. Out-of-date processor fabrication blocks were utilized to develop semiconductor LOC platform. In recent years, a polymer-based LOC product emerged in this area. The most common-used material is transparent polydimethylsiloxane(PDMS). Silicon wafer, PDMS and glass, these materials constitute LOC fabrication platform.

As dimensions scale down to microns, heat transfer, diffusion rate and reaction rate goes up, traditional limits on biological process or chemical reactions are eliminated. This nature features Lab-on-chip technology with small sample requirement, high sensitivity, and fast response time. A miniature idea of assembling multifunctional unit onto one chip also brings a highly portable device to public attentions. As a result, chemists and biologists have gained interest in the rapid growth of microfluidic system in recent years.

Practical LOC technologies are developed in biochemistry analysis (1), cell manipulation (2), and real time reaction rate analysis (3), drug discovery (4), etc.

1.2 Fluid control issues in LOC device

The creation of LOC products is still challenging due to a variety of technical limitations. Among them, fluid manipulation often becomes a central source of complexity and mechanical failure. For LOC products, most common used driving force is pressure. External pumps provide driving force for fluid motion inside LOC product through connected tubes. Complex external pump and tubing system have created bad portability, and render lab-on-chip technology to chip-in-lab devices. In the meantime, fluid control is also required by LOC products, like sample injection (5), establishing gradients (6), compound buffer delivery (7), micro total analysis systems (8) and complex fluid routing (9). These applications often involve complex fluid matrix and sequential buffer delivery. Especially in analytical implementations, precise control on fluid motion directly relates to accuracy of analysis process and system reliability. For precise-control purpose, a complicated pressure regulation system is assembled between pressure pump and LOC products.

To summarize, increased demand for fluidic control has resulted in complicated chip designs and has increased the use of bulky external pressure sources. Complex external

pump and tubing system have created bad portability, and render lab-on-chip technology to chip-in-lab devices. The solution to this problem is micro-pumps that can be integrated into the microfluidic chips and can be controlled by portable computer components.

1.3 Increasing Demands of micro-pump

Due to the bulky volume and bad portability, chip-embedded micro-pump developments draw much attention from engineers in recent years. To deliver substantial pressure difference and mass flow, two types of pumps are proposed in current research. They are manually divided into two categories, displacement pumps (10), and kinetic pumps (11).

Displacement pumps, also known as mechanical pumps, involve an oscillating boundary surface and deliver mass flow periodically. Generally this surface is made of silicon, glass or plastic, with fixed edges. A driver moves this membrane back and forth and change chamber's volume alternatively. Fluid is drawn into the chamber in an expansion step (volume increases), while discharged in a compression step (volume decreases). Check valves are placed to prevent back flow in displacement pump. Displacement pump was first proposed by Harald van Lintel (12) as early as 1988. It has been well developed and featured with high flow rate delivery. However, the displacement pump requires at least two layers fabrication process. The maximum layers of reported displacement pump are seven (13). A multiple layers fabrication leads to tedious work and precise fabrication

control. Generally this process is not applicable in manufacturing setting and limits implementation of displacement pump. Besides, presence of oscillating part often causes structural failure due to friction or elasticity loss (14), especially for those high through put pumps.

On the contrary, kinetic pumps convert other energies into kinetic energy to create momentum in the fluid, resulting in a continuous flow with enough force to overcome the viscous force in microfluidic systems. The most common types of kinetic pump are centrifugal pumps or microturbines. But the applications of these pumps are restricted by fabrication techniques. Alternative kinetic pumps have been extensively studied to develop the electrohydrodynamic pump (15), which is based on Coulomb force acting on free charge in fluid. It requires inhomogeneity to create space charge, which can be induced from inhomogeneous fluid or free charge injection; electrokinetic pump by Seiler et al(16), magnetohydrodynamic pump by Eijkel et al(17), which is utilizing magnetic field to induce Lorentz force on ions in solution; thermomagnetic pump by Pal et al(18), electro wetting pump by Moon(19) and electrochemical pump(20).

1.4 Introduction to Electrokinetic Pump

Among these kinetic pumps, electrokinetic pump has a relatively good performance regarding on generated pressure, flow rate and fabrication cost. Typically it uses

dielectrophoresis (DEP) and electro-osmosis (EO) to create fluid flow. DEP utilizes a non-uniform electric field to exert a force on dielectric particles while EO is related to counter-ion drag force from a parallel electric field. Here we provide more details on electroosmotic pump as it's directly related to our work.

EO phenomenon was discovered almost 200 years ago (21). Surface charge appears spontaneously when contacting with liquid phase and further pulls counter ions in bulk liquid near to surface. This thin layer of ions is called electrical double layer (EDL) featured with thickness characterized by Debye length. Tangential electric force is applied on this layer to move along with electric field, which creates drag force on bulk fluid. Researchers haven't applied EO phenomenon to micro-pumps until the past decades. An EO pump packed with silica particles was presented by Zeng et al, which acquired a flow rate of 0.8mL/min and a pressure of 1 atm backpressure. Another type of EO pump with non-packed channel was developed by Chen and Santiago (22) but the working pressure generated by the micro-pump significantly reduced due to the relatively large dimension and low resistance. In contrast to mechanical pumps, EO pumps can provide much smaller flow rate, down to milliliters per minute, which can be used to precisely control sample injection.

1.5 Drawbacks of Current Electrokinetic pump

Even though EO pumps were widely studied in recent years, most of them still suffer drawbacks from system design. Most of EO pumps have tedious packing procedures to increase output pressure. This packing procedure in EO pump fabrication leads to an increase in fabrication expense and quality variations due to the limitation of packing technique. Moreover, particles, polymers, and cells tend to block packed channels and affect the working capacity of the EO pump. This bulky design also limits integrations of EO pump onto other microfluidic system.

For those non-packed EO pumps, there is a high voltage requirement to generate enough pressure difference, creating a high current density across the channel. A direct contact between highly charged electrodes and fluids results in surface reactions that cause problems like, cell or macromolecule damage (23), pH variation (24), electrothermal flow (25)), and Joule heating (26) and electrode decomposition. It also suffers contamination issues as bio-samples are exposed to electrode surface, as well as atmosphere. All these disadvantages restrict EO pump applications into a narrow area in biomedical research.

Recently, a contactless DEP device associated with DI water electrode was presented by M.Sano et al ((27)) which includes isolated electrodes along flow channel. This idea may provide a new aspect in EO pump design without problems caused by direct-contact.

1.6 New strategy in pump design

In our work, we came up with a novel metallic electrode that utilizes contactless EO phenomenon to create a micro-pump in a LOC device. Electrodes are isolated from working fluid by a thin layer of PDMS. This concept successfully eliminated drawbacks from traditional EO pumps, such as electrode decomposition, bubble generation or pH variation at electrode surfaces, contaminations and sample damage caused by direct current across the channel. Furthermore, we used gallium metal injection in electrode fabrication to further solve the connection and electrode evaporation problems associated with using DI water in the charged channels. Due to the low viscosity nature of gallium metal, liquid phase, we are able to shape metal electrodes in three dimensions by injecting gallium into confined electrode channel. Sealed gallium electrodes eliminate potential disconnection issue caused by water evaporation or trapped air bubbles. By presenting simple engineering approaches to characterize its working capacity, we were able to further its applications in other microfluidic device with lower fabrication cost and improved portability. A closed circuit loop channel was designed to quantify the flow rate purely generated by this EO pump. Next, the pumping unit was added into a T-shape channel for further characterization under small hydrodynamic resistance case. Finally, we demonstrate two potential implementations of gallium pump serve for fluid manipulation and plug generation purpose, individually.

Chapter 2 Theory

2.1 Electric-Double-Layer model and Electro-Osmotic flow

When an electric field is applied across a microfluidic channel, the interface between the wall and electrolytic solution polarizes with a fixed net electric charge. This mobile layer of ions is known as the electric double layer (EDL). The net charge in the EDL generates Coulomb force on the fluid and is the driving force for EO flow. The EDL plays such an essential role in EO phenomenon that modeling EO flow profiles commonly varies according to the EDL's length scale. Within the region of the EDL, also known as Debye length, we usually derive the unidirectional solution from Navier-Stokes equation. Assuming applied electric field is uniform inside the EDL and there is no external pressure gradient, associating with the Poisson equation, we simply arrive at

$$0 = \eta \frac{\partial^2 u}{\partial y^2} - \varepsilon \frac{\partial^2 \varphi}{\partial y^2} E_w \quad \text{Eq.1}$$

where the first term on right hand side is shear force or viscous force and the second term is Coulomb force. Terms η, ε, ϕ and E_w denote viscosity, permittivity, electric potential, and the tangential component of electric field respectively. By integrating with a no-slip boundary condition and ϕ=0 outside of the EDL, Eq.1 becomes

$$u_{in} = \frac{\varepsilon E_w}{\eta}(\varphi - \varphi_0) \quad \text{Eq.2}$$

where ϕ_0 is wall potential. Eq.2 is called the inner solution for the EDL region.

Normally Deb ye length is on the nano scale. For phenomenon visible under microscope,

the outer solution models the bulk fluid motion with the assumption that the EDL is finite. If the Debye length is much smaller in comparison to the microchannel's width, it generates the *Helmholtz-Smoluchowski* equation,

$$u = -\frac{\varepsilon E_w}{\eta}\varphi_0 \quad \text{Eq.3}$$

by making ϕ equal to 0. Eq.3 is the new boundary condition for bulk flow at wall. By replacing ϕ_0 to a measureable parameter ζ, known as zeta potential, we have

$$u_{out} = -\frac{\varepsilon E_w \zeta}{\eta} \quad \text{Eq.4}$$

This is a plug flow with equal velocity along the y-axis, but it only happens under a hydrodynamic load-free circumstance.

2.2 Linear Combination of "Frustrated" Flow

Equation above describes EO flow without impacts from other fluid properties. For EK pumps, which work against hydrodynamic resistance, a counter pressure resulting from viscosity must be considered. A combination of EO flow and counter pressure driven flow is called "frustrated" flow, shown in *Fig.1*, and is modeled by Rice et al (28). For 2D flow profile, with channel's width much larger than height,$\omega \gg 2d$, calculated EO and pressure driven flow rates are shown as Eq.5 and 6.

$$Q_{\mathrm{EO}} = -2\omega\frac{\varepsilon E_w \zeta}{\eta} d \quad \text{Eq.5}$$

$$Q_{\mathrm{P}} = -\frac{2\omega}{3\eta}\left(-\frac{\partial p}{\partial x}\right)d^3 \quad \text{Eq.6}$$

The full flow profile is a linear combination of these two equations.

$$Q = -2\omega\frac{\varepsilon E_w \zeta}{\eta}d - \frac{2\omega}{3\eta}(-\frac{\partial p}{\partial x})d^3 \quad \text{Eq.7}$$

The first term in Eq.7 is the EO flow rate while the second term is the counter flow rate resulted from hydrodynamic resistance.

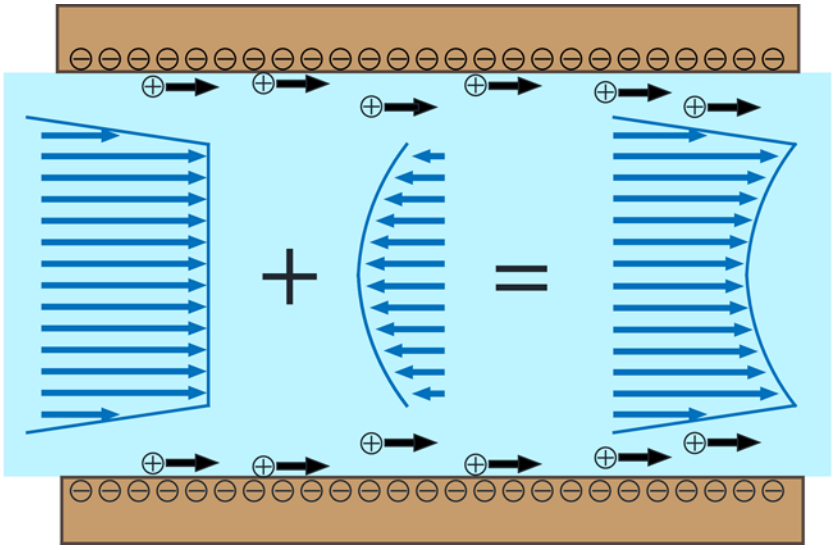

Fig.1 Illustration of "frustrated" flow. Full flow profile is a linear combination of EO flow and Poiseuille flow. Electric field forces counter ions to move along the field direction like slippery boundaries. Movement of boundaries creates drag force to drive EO flow. Note that the thickness of EDL is enlarged to show.

2.3 Model for "Loop": work against certain resistance

In our first experiment, a closed circuit design named "Loop" will be introduced. EK pump creates a pressure difference when an electric field is applied and drives fluid circulation inside the loop. In this case, fluid motion is purely driven by EK pump against hydrodynamic resistance in frustrated flow profile, which is represented in *Fig.1*.

Corresponding net flow rate Q is determined by Eq.8. Within a closed circuit, mass balance requires flow rate (Q) to remain constant, which is also characterized by Eq.8. ΔP is the total pressure generated by EK pump to drive fluid along the loop, Q is net flow rate from linear combination of EO flow and counter pressure flow, R_h is hydrodynamic resistance of flow channel which is given by Eq.9 for circular cross-section with radius of r and Eq.10 for rectangular cross-section with height of h,

$$\Delta P = QR_h \quad \text{Eq.8}$$

$$R_h = \frac{8\eta \Delta L}{r^2 A} \quad \text{Eq.9}$$

$$R_h = \frac{12\eta \Delta L}{wh^3\left(1-\frac{0.63h}{w}\right)} \quad \text{Eq.10}$$

Replacing E_w in Eq.7 with definition $\Delta V/\Delta L_1$, and changing $-\partial p/\partial x$ to $\Delta P/\Delta L_2$, rearranging gives

$$\Delta P = \frac{6\omega d\varepsilon\zeta \Delta L_2 R_h}{2\omega d^3 \Delta L_1 R_h + 3\eta \Delta L_1 \Delta L_2}\Delta V \quad \text{Eq.11}$$

where ΔL_1 is the separation between two electrodes and ΔL_2 is total length of the loop.

2.4 Model for "T-shape": small hydrodynamic resistance case

To analyze the effect of EK pumps on the "T-shape" channel design, we start from Eq.5. In this case, counter pressure is caused by external pressure source instead of working against hydrodynamic resistance. For the inlet stream where the EK pump is off, the driving force is purely external pressure. Flow rate Q_P is given by $\Delta P/R_h$ rather than

Eq.6, while Q_{EO} is still determined by Eq.5. When both external pressure and gallium pump are present, the net flow rate for inlet stream is a combination of "EO" flow and pressure driven flow. In the case where we adjust the gallium pump to generate pressure equal to external pressure near pumping area, the net flow rate becomes zero. By setting Eq.5 $=Q_P$, $E_w = \Delta V/\Delta L_1$ substituting Q_P and rearranging, we get an expression that describes how the pumping pressure is related to applied voltage

$$\Delta P = \frac{2wd\varepsilon\zeta R_h}{\Delta L_1 \eta}\Delta V \quad \text{Eq.12}$$

where R_h is calculated based on T-shape design. Eq.11 and 12 provide linear relations between applied voltage and pressure for both experiments. The pumping pressure is determined by channel structure, surface properties, media permittivity and applied voltage. The EK pump's performance is restricted to its structure; smaller dimensions create larger pressures, with certain working media and voltage.

2.5 Modifications on Contactless Design

In our work, the new created contactless micro pump shares similar electro osmotic principle with traditional EO pump modeled by Eq,11 and 12. However, due to the existence of PDMS membrane, electric field along flow channel is hugely reduced as a dramatic potential drop occurring across PDMS membrane. Thus, a potential loss factor is required to adjust existing model to represent high resistance of isolation membrane. Here we apply a simple ohm's law to calculate approximated potential drop ΔV along the

flow channel. Resistances are calculated from Eq.13, where ρ is resistivity, L is length of membrane and A is cross-section area. The corresponding ΔV is given by Eq.14,

$R = \rho \frac{L}{A}$ Eq.13

$\Delta V_{DI} = \Delta V_{total} \frac{R_{DI}}{R_{total}}$ Eq.14

Permittivity is also an important factor for pumping performance optimization. Additives that increase the dielectric constant, like zwitterions (29) are able to improve EK pump performance by 3 fold. And for biology or analytic chemistry purposes, designing buffers with higher permittivity and biocompatibility will be a key element in contactless micro-pump optimization. However, adding solute to increase dielectric constant may also result in increased viscosity. Although viscosity is not a factor when trying to output maximum pressure and reduce flow rate to zero, it does influence hydrodynamic resistant and net flow rate in other pumping events.

Although conductivity does not appear in any above equation, it impacts other parameters that determining net flow rate and pressure. Zeta potential decreases when conductivity goes up, resulting in lower pump performance. Additionally, high conductivity can result in excess counter ions aggregation near electrodes and formation of counter electric field, creating a “screening effect” at the solid-liquid interface. Free charges in buffer solution adhere to PDMS layer near electrodes by electrophoresis, which shield electrostatic field

along the channel and reduce its magnitude. It is an unavoidable drawback by contactless design, which narrows contactless EK pump applications to low conductivity buffer. Due the "screening effect", Eq.11 and 12 must be modified as the real electrostatic field is less than $\Delta V/\Delta L_1$. No mathematic model has been established for this so-called "screening effect", and its dependence on buffer conductivity, electrodes structure and permeability of the membrane material makes it a complex problem. However, the electrode structure and PDMS permeability is known and fixed. This model is simplified to one variable, conductivity, which is supposed to reduce electric field strength linearly.

Chapter 3 Materials and method

3.1 Gallium pump structure

We name this pump design as contactless pump because a thin layer of PDMS, 45μm, separates electrodes from flow channels, shown in *Fig.*2. The electrode channel was designed to be 900μm wide to provide relatively uniformed electric field vertical to PDMS membranes. Symmetric electrodes are placed on both side of flow channel to enhance electric field magnitude. Two parallel sets of electrodes were fabricated to induce potential drop along with flow channel direction to induce tangential electric field. Note that separation distance between two parallel electrodes will influence field strength. However, for fabrication concerns and practical setup, this distance should be large enough to avoid electrode short-out. The electrode designs differ in the injection stream width due to optimization purpose. As low viscosity of gallium metal in liquid phase, metal injection is easy to perform even in micron scale structures. But it also leads to higher requirement on injecting operation to fabricate uniformed electrode without trapping air inside. A thinner injection stream increases resistance and reduces air bubbles inside electrode. While pumping capability remains constant as long as the dimension of electrode remains constant.

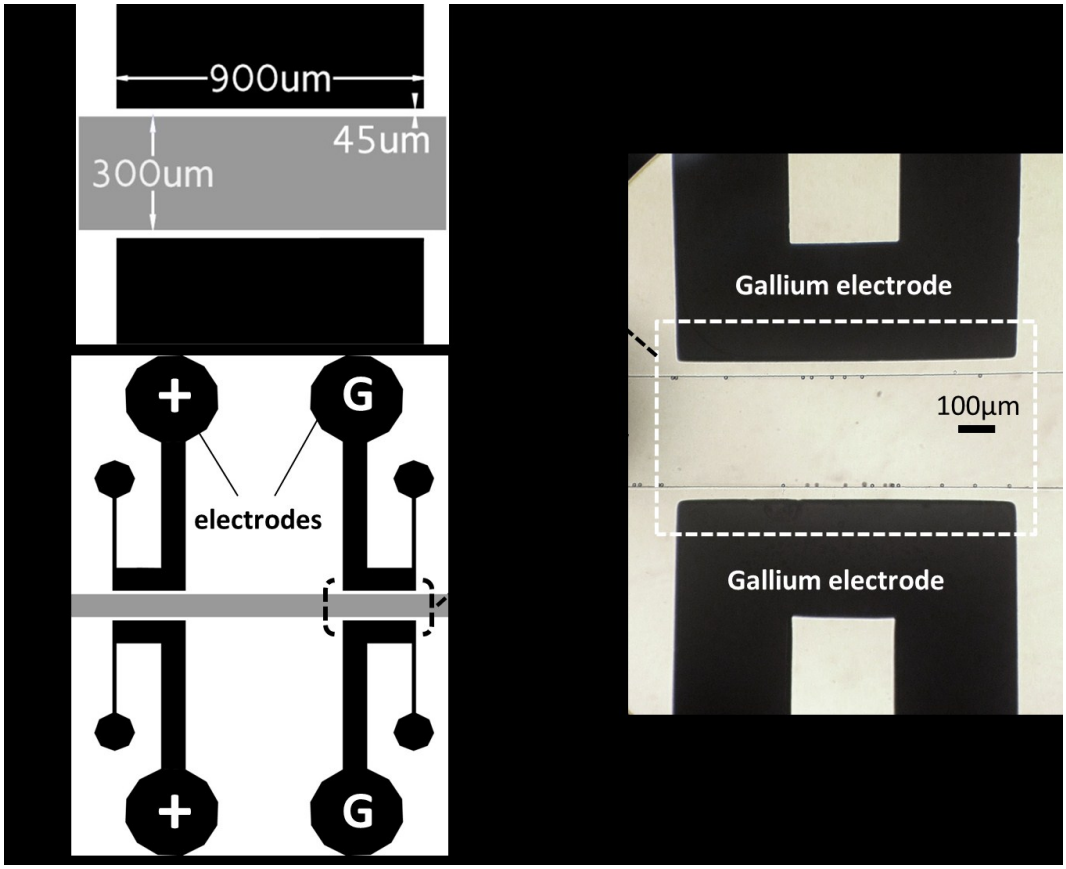

Fig.2 Structure of contactless gallium metallic pump. (a)Detailed dimension of gallium electrodes. (b)Enlarged image of PDMS layer, which largely affects electric field strength due to its resistance. (c)Dimension of pump structure and separation distance applied in follow chips.

3.2 PDMS device fabrication

Chip fabrication was performed in common soft lithography process. Clear field, known as negative, masks were designed in AutoCAD and printed on transparencies (Plotting, Fineline imaging, CO). A Silicon wafer was preheated on hot plate at 200℃ for dehydration for 10min. The wafer was coated with photoresist SU-8 3050 to 50μm

thicknesses. This thickness is optimized for both performance purpose and practical purpose. If channel's height goes up with constant separation distance, two channels may collapse. But a decreased height also influences chip performance as electrical resistance is increased. Coating process was performed on spinner with 500rpm and 3000 rpm steps, referred manufacturing protocol. After 30min soft baking, wafer was exposed to UV light under pre-designed mask. Post baking was also required before final development step. Developing lasted for 7-8min to wash out unlinked photoresist. Geometries and thickness were measured before use.

When a wafer mold was completed, liquid phase PDMS and crosslink agent (RS Hughes Co Inc. USA) in a ratio of 10:1 were mixed by a planetary mixer (ARM 310, Thinky Co. Japan) at 2000 rpm/min for 30s, then directly poured onto silicon wafer mold. Degasing process lasts 10-15min in a vacuum chamber. Degased PDMS was cured under 85℃ for 30mins. If smaller features are included, degasing time should be extended to remove small bubbles trapped in these gaps. Inlets and outlets were punched on PDMS by 0.75 mm Uni-core (Harris, Ted Pella, Inc. USA) and connecting holes for electrodes were performed in 0.75 mm size. Cover glass (Fisher finest, USA) was cleaned by Acetone and IPA and dried by nitrogen air. Surface treatment was conducted by oxygen plasma (BD-20, Electro-technic Products Inc. USA) for 10s. Then the glass was bounded with

PDMS and baked at 85℃.

3.3 Gallium electrodes fabrication

Gallium injection to create electrodes was performed after device fabrication. Gallium metal (Sigma-Aldrich USA) and the PDMS chip were heated on a hot plate to a temperature above 29.7℃. A standard syringe pump was used to inject liquid phase gallium into electrode channels. Due to gallium's low viscosity, 1.37mPa·s (30), no surface treatment was required. If electrode channel is not filled properly, air bubbles may be trapped inside. In this case, increase internal pressure through syringe pump to remove trapped air. Copper wires were plugged into inlets holes after injection to seal electrodes and create a voltage source connection point. A resistance meter was used to determine if the electrode channel filled completely.

3.4 Reagent preparation

10μm green fluorescent plane silica nanoparticle solution (2.5%, Corpuscular Inc.) was dilute in 1.5 ml DI water before use (concentration of 0.08%). Conductivity of suspended particle solution is 2μS/cm. The red and green fluorescent solutions ($2.8*10^{-4}$mg/ml) were made by adding 100μl stock solution (0.01mg/ml) (Alexa Fluor, Sigma) into 4ml DI water with a conductivity of 1μS/cm.

3.5 Automation of power distribution system

To facilitate experiment operation and automation process, a LabVIEW based DC power distribution interface was established here to achieve independent control of each pumping, shown in Fig.3. LabVIEW (2009, National Instruments, TX) was programmed to send 5V signal to individual port on USB I/O hub (24R Elexol, Australia). Customized PCB board associated with USB I/O, Fig.3(b)(c), was able to amplify this signal to 12V, which consequentially activated individual reed relay(DAT, Digikey, MN) assembled on breadboard Fig.3(e). When activated, high voltage signal from DC power supply (PS325, Stanford Research System, CA) was able to pass through the relay and start pumping process Fig.3(f). With this manual assembled system, independent control on each gallium pump became possible. Then sequential activation of pumps and pumping time could be regulated by LabVIEW programing. This system not only facilitates current experiment operations, but also provides a potential solution for complex designed pumping network after scale up. User-friendly software interface will expand its market even into non-scientific background end-user, which definitely boosts commercialization of microfluid products.

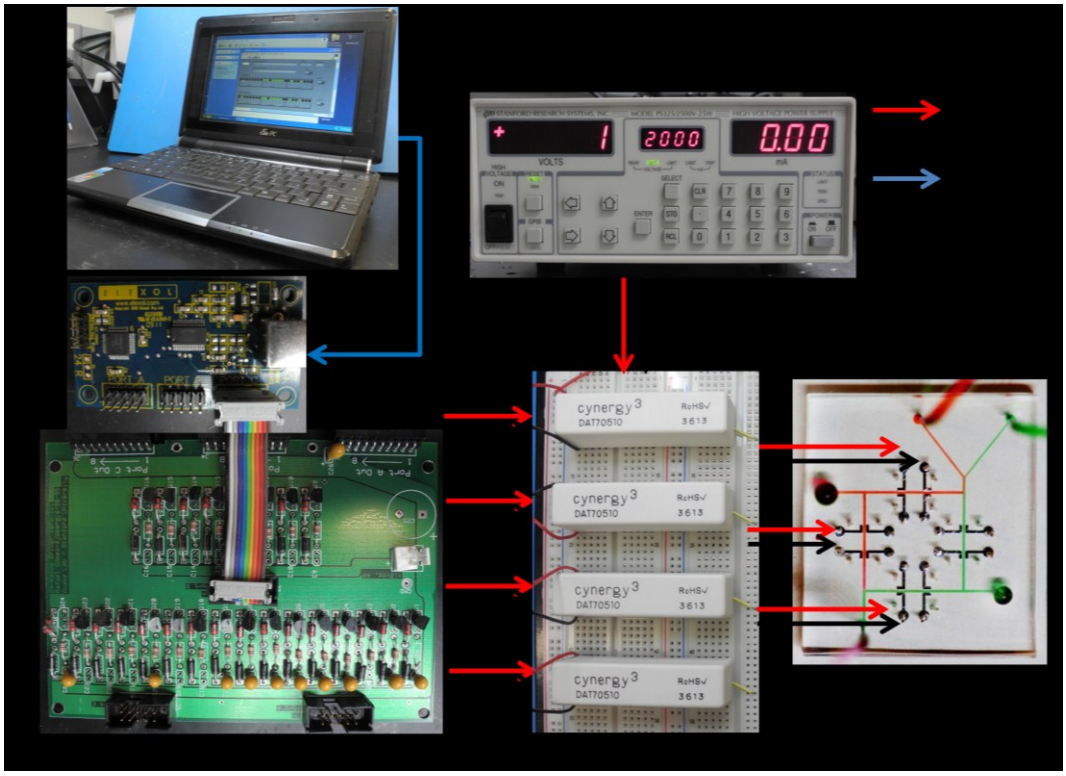

Fig.3 LabVIEW controlled power distribution system for multiple pumps activation. (a)LabVIEW provided visual control panel on laptop and regulated signals transmitting. (b)(c)USB I/O and PCB board were connected by ribbon cable to amplify signal output for relay activation. (d)DC power supply continuously provided high voltage source to relays. (e)Relays were assembled on breadboard and connected to power supply, PCB board. These relays served as pump switches when received an activation signal exceeding its switch-on limit. (f)The other ends of relays were directed to multiple gallium pumps. Each relay controlled one pump independently Chapter 4 Result and discussion

Chapter 4 Result and Discussion

4.1 General performance characterization with “Loop” design

We resuspended silica nanoparticle solution before injected this homogeneous suspension into flow channel, either by a syringe or external pump. Outlet was sealed after loading process to degas. Then we sealed inlets and established an external load-free fluid circuit, shown in Fig.4(a). Copper wire directed high voltage DC power source to pump1 electrodes to activate gallium pump. Particle movement at the far end (pump2 area), which represented fluid motion, was captured by an inverted confocal microscope (Nikon, NY). The reason for acquiring image near pump2 is to minimize the dielectrophoresis effects on silica particles and misrepresentation of flow rate. We turned on a high speed camera, (DS-Qi1Mc, Nikon), to record particle’s motion at no-delay model (0.1s/frame) after 10s since pump was on. Duplicated experiments were repeated several times under each applied potential. Acquired videos were further analyzed by NIS Element software (Nikon) to measure moving distance between two time points. Based on these data and channel dimension, we can calculate particle velocity, which represented flow rate generated by gallium pump and a combination of “frustrated” flow.

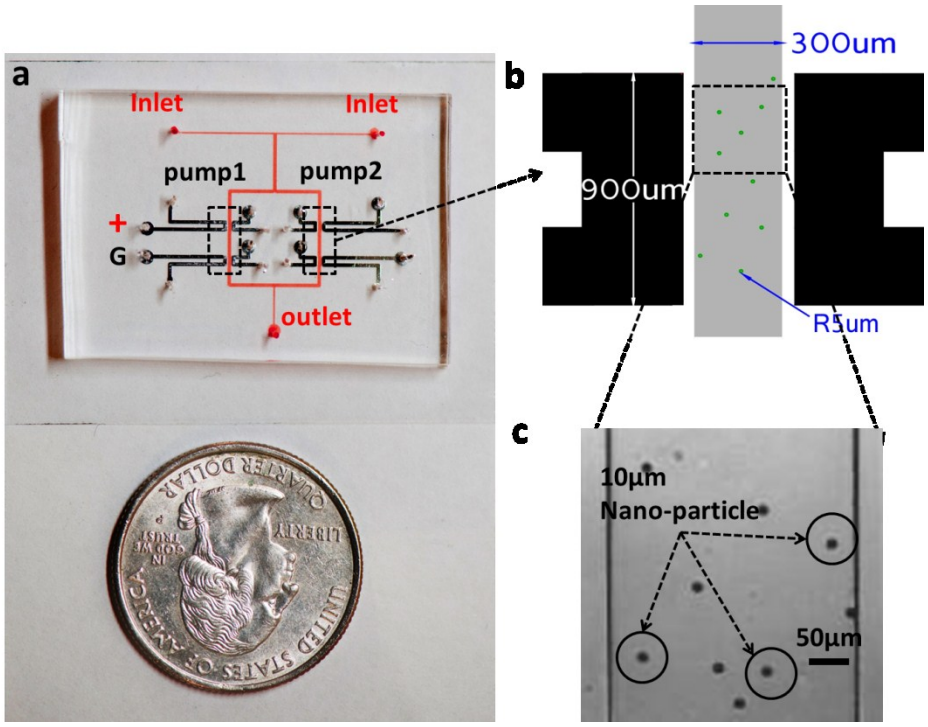

Fig.4 "Loop" experiment setup. (a) Represents a completed real image of "Loop" design. (b) Local illustration of electrode structure. (c) Real image of silica particles under bright field.

Here we chose plain surface silica nanoparticle to reduce solution's conductivity as influences from screening effect should be minimized. However, tested conductivity of particle suspension (2μS/cm) is still slightly higher than normal DI water (<1μS/cm). Besides, neutral particle also results in larger drag force from channel walls and bottom surface as there is no free charge to prevent it from sticking. So it's quite reasonable to assume an underestimation of flow rate, due to a combining result of screening effect and drag force. Especially under lower range of applied potential, this underestimation will be

more obvious. Due to the existing of stationary drag force on silica particles, certain flow rate must be reached before the shear force is sufficient to overcome stationary drag force. This force balance will be interpreted as no obvious particle movement under lower voltage until applied potential exceeds threshold value. This assumption was also supported by the following data plot Fig.5.

To achieve more accurate flow rates, each measurement was repeated several times under same voltage and average velocities were calculated to reduce system error and data divergence. Using Eq.8, we derived net flow rate and corresponding pressure created by single EK pump, shown in Fig.5. The linear fit was analyzed by OriginLab (Version 8.6, OriginLab, MA).

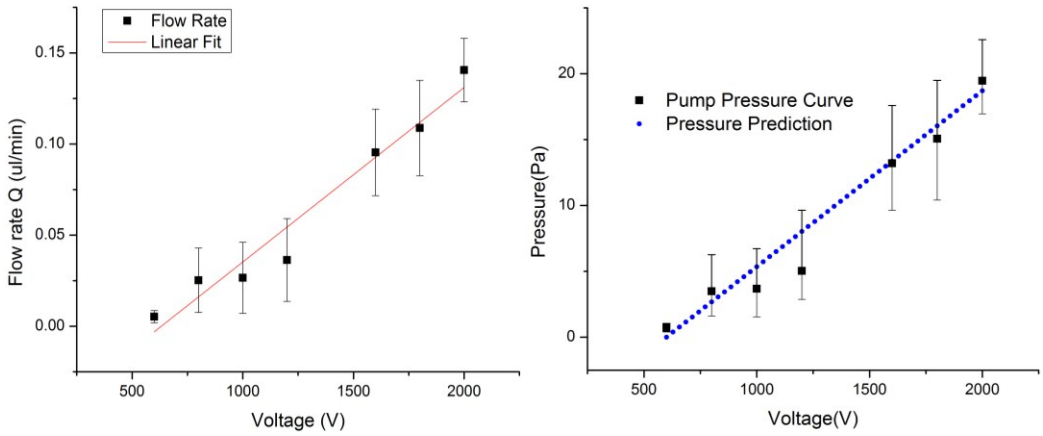

Fig.5 Flow rate and pressure plots versus potential. (a) Flow rate calculated from average velocity versus applied voltage. (b) Pressure generated by gallium pump under different potential with error bar. The

linear prediction is derived from Eq.11 with modification.

From Fig.5(a), OriginLab predicts a linear fitting curve for average flow rate data with R-square value 0.95, which means a good fit. It's safe to draw a conclusion that measured flow rate increases linearly as applied voltage goes up. As we expected, there was no significant difference in flow rates below 600V and particle remained stationary until 600V was applied. Shown in Fig.5(a), maximum flow rate under 600V is around 0.005μl/min, which is relatively small and difficult to notice. It goes to 0.14μl/min as potential increases from 600V to 2000V.

The corresponding pressure curve is calculated from Eq.8 and plotted in Fig.5(b). A theoretical curve of pumping pressure indicates estimated pressure generated by gallium pump. Parameters are substituted into Eq.11 to calculate the slope of linear prediction. By taking potential loss in contactless design into consideration, ΔV is replaced by ΔV_{DI} in Eq.14. We further insert an underestimation factor into this expression to represent the impacts from drag force and screening effect. Note that this modification factor is estimated from experimental observations rather than theoretical calculation as no mathematic model currently available for screening effect. Finally we derive the theoretical prediction shown in Eq.15. The slope of 0.417 comes from Eq.11 and the potential loss factor of 0.032 is derived from Eq.14. Underestimation factor, 0.032*600,

is an approximation from collected data, which corresponding to the observation under 600V.

$$\Delta P = 0.41746 * (0.032\Delta V - 0.032 * 600) \quad \text{Eq.15}$$

In Fig.5(b), an average pumping pressure of 20Pa is achieved when 2000V applied, while individual point reaches a maximum pressure of 23Pa. We include y-axis error bars to represent data divergence. The maximum pressure variation is acquired under 1800V, which is $\pm$4.5Pa from standard value 15Pa. According to experiment data and observations, we drew a conclusion that these variations of pumping performance mainly come from structure deformation and resistivity alternation occur at PDMS membrane. In electrode fabrication process, we utilized liquid metal injection technique to build three dimensional gallium electrodes. One of the drawbacks of injection technique is lack of control on internal pressure, which means internal pressure of electrode may vary according to fabrication process. Consequently, PDMS membranes experience a diverse degree of elastic deformation. Measured PDMS membrane thickness between electrodes and flow channel varies from 37μm to 42μm, respectively. This deformation is believed to cause data divergence due to a resistance change in Eq.14.

Regardless of data variation, our mathematic model provides a relatively accurate prediction on pumping performance against certain hydrodynamic resistance in a range of

600V to 2000V. For theoretical prediction under 600V, this model losses its accuracy and gives meaningless negative approximation. As drag force and screening effect become dominant in low velocity field, pressure gradient created by gallium pump is insufficient to overcome stationary drag force and drive particle to move. When voltage falls below 600V, particle simply remains stationary regardless of actual flow rate. Flow rate within this range is disregarded in our theoretical model, and represented as underestimation factor.

Note that these pumping pressures are achieve without packing procedure, which is widely utilized in traditional electrokinetic pump to increase generated pressure. General methods are performed with micron to nano scaled silica particles or polymers to form compact porous structure. Principle behind this structure is a dramatically increased hydrodynamic resistance, which leads to higher output pressure up to MPa. But porous structure also reduces flow rate in the same degree. So it's a trade-off between pumping pressure and flow rate according to application purpose.

4.2 Maximum capability characterization with "T-shape" design

To double check the working capacity of gallium pump, a T-shape chip (Fig.6) was fabricated to calibrate its relative parameters. Fabrication process was same to former experiment and well described in chip fabrication section. Channel's height was same to

“Loop” design. 4ml wells served as fluid reservoirs on the external pressure source. Each well was filled with prepared green and red fluorescent solutions respectively. Solution with fluorescent dye has a conductivity of 1μS/cm. Microbore tubes (Cole-Parmer, 0.02’’ID, IL) were connected to fluid reservoirs to direct solution into microfluidic chip. Fluorescent solutions were driven by a small external pressure and entered a T-shape channel through inlets. Degasing was performed by sealing outlet. After degasing, seal was removed and allowed to flow solutions into outlet. Alternative lasers source with 488 and 594 wavelength excited fluorescent dyes. Emission signals were captured by high speed camera on confocal microscope. To establish an interface that indicating fluid motion, we adjusted pressure gauges to balance flow rates in two inlet stream. Under identical flow rates, a two-color interface was formed at the central line of flow channel, shown in Fig.6(b). After interface balancing, we further reduced external pressure to a lower range while kept interface remain in the middle. This range should be within the working pressure of gallium pump. When gallium pump1, Fig.6(a) was activated, it created counter pressure against external pressure source and consequently altered interface position. Under certain voltage, the counter pressure was large enough to balance external pressure, known as $P_{ek} \geq P_{ex}$. As a result, liquid-liquid interface would shift to left. If $P_{ek}=P_{ex}$, net flow rate of left stream is zero, which corresponding to stationary position of the interface, shown in Fig.6(c). However, pressure information

near inlet stream is not available under current setting. Instead, flow rate Q_P can be acquired from different ways easily. Here we induced fluorescent nanoparticles into the other stream to calibrate flow rate of right stream, which is equal to left stream. The reason for not inducing particle into left stream directly is to minimize screening effect. Alternative method would be measuring velocity of trapped air bubble or meniscus inside an extended tube which is attached to outlet. From measured flow rate, we were able to calculate ΔP between outlet and inlet stream, from where P_{ek} was determined.

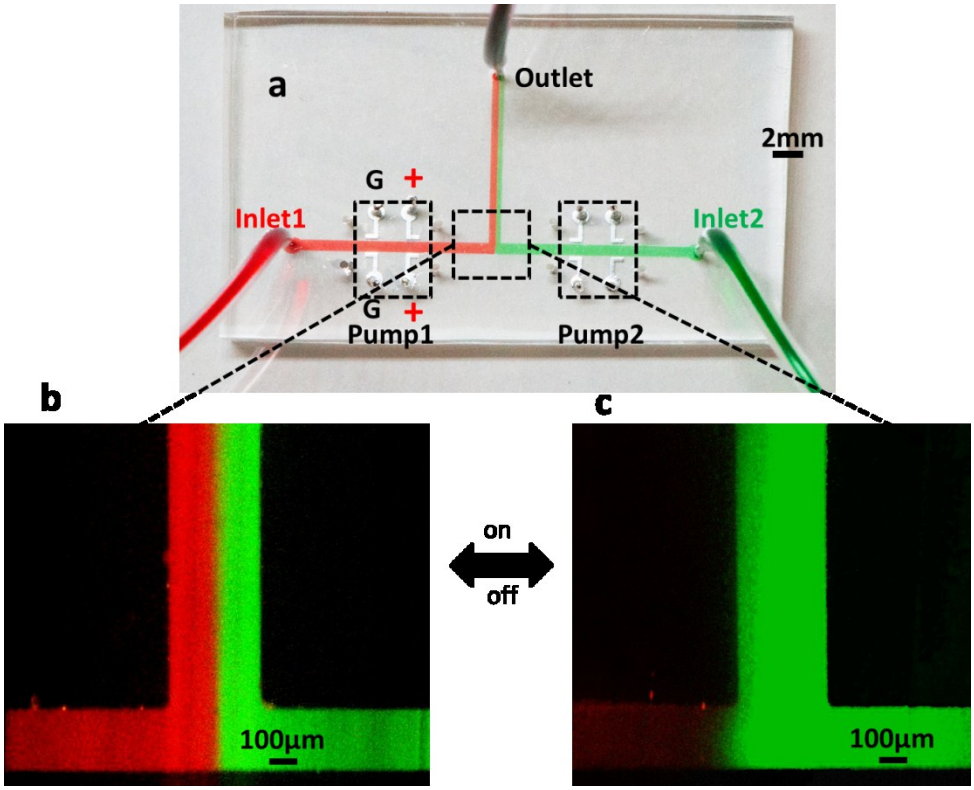

Fig.6 "T-shape" test setup. (a)Inlets were filled with colors to represent excitation of fluorescent dyes. Flow rates of these two inlets were regulated by external pressure source. In this experiment pump1 was

connected to power supply while pump2 remain still. (b)Interface kept its position when both pumps were turned off. Diffusion effect at interface increased along main channel due to a small flow rate. (c)When pump1 was activated, red fluid was driven backward which caused interface shifted to left.

Eq.12 summarizes this calibration method and provides theoretical estimation of electrokinetic pressure, P_{ek}, created by gallium pump. With similar reasons, Eq.12 also requires modifications to represent realistic performance of contactless pump. By inducing potential loss factor and underestimation factor, we derive Eq.16 in a similar format.

$$\Delta P = 1.0895 * (\Delta V * 0.032 - 550 * 0.032) \quad \text{Eq.16}$$

As electrode's dimensions remain constant, potential loss factor remains unchanged. Potential difference along the flow channel comes from $\Delta V * 0.032$, proving that our theoretical model is acceptable. However, underestimation factor from collected data gives number of $550 * 0.032$, instead of $600 * 0.032$, which is slightly lower than former approximation. As difference in drag force for these two experiments is relatively small, it is safe to assume that this reduction mainly comes from a decrease in solution conductivity. In other words, it results from variation in screening effect magnitude. But this assumption is lack of experiment backup, to setup accurate mathematical model to study influence of screening effect, further researches are needed.

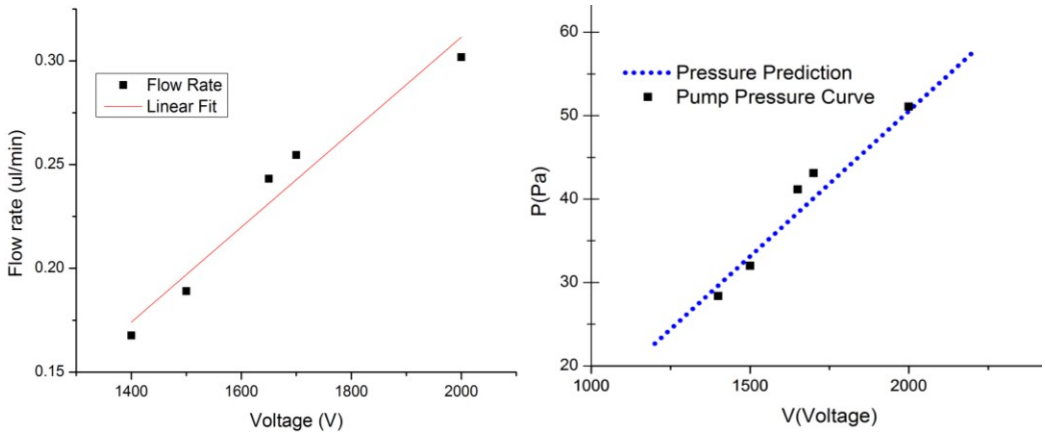

Fig.7 Pumping flow rate and pressure versus applied voltage. (a)Plot of flow rate generated by gallium pump in T-shape device with linear fit curve. (b)Pressure data collected from T-shape device is compared with theoretic linear prediction.

Fig.7 provides characterized parameters in T-shape design. Here "EO" flow rate represents working performance of gallium pump without hydrodynamic resistance, which has higher efficiency under same voltage. Flow rate is around 0.17μl/min at 1400V and linearly increases with applied potential. A 0.3μl/min flow is balanced by 2000V, which is the maximum value achieved in this experiment. OriginLab fitting analysis gives an R-square value of 0.94, means a relatively good fit among data points. Fig.7(b) is a comparison between theoretical prediction and realistic pumping data. Pumping pressures range 28Pa at 1400V to 51Pa at 2000V. Because in T-shape design, gallium pump only carries a small part of fluid near pumping area while the rest fluid in left stream remain stationary, loading of hydrodynamic resistance is neglectable. The net flow

rate generated by gallium pump is dominated by “EO” flow, which is balanced by external pressure. In other words, with T-shape design, gallium pump is working without resistance loading and reaches maximum pumping capability.

Our mathematic model offers a good approximation on pumping pressure within a range of 1400V to 2000V. We can expect loss of accuracy again in low potential range. Here according to Eq.16, upper limit of this underestimation range is around 550V, which means flow rates generated by 550V or below, are treated as zero due to the non-neglectable drag force and screening effect. Note that this underestimation factor can be further minimized by replacing particle tracking method with other potential flow rate measurements where drag force is no longer exist.

4.3 Potential optimizing strategies

Working capacity of contactless gallium pump depends on pump structure, dimensions, resistance load and conductivity of working solution. These effective parameters fall into three modification factors in pump characterization curve. The first factor is slope, which is influenced by hydrodynamic resistance, flow channel dimension and working fluid selections. It’s mainly pre-determined by experiment design. As we mentioned in former section, a practical method to increase pumping performance is proposed by David by using zwitterions to increase working fluid permittivity. (8).

The second factor is potential loss factor, which impacts actually potential difference to drive “EO” flow. Electric conductivities of materials play a significant role in this model. In our mathematical model, resistivity of PDMS and DI water is set to be 2e9Ω/cm and 5e5Ω/cm. To our knowledge, PDMS cured with crosslink agent hasn’t been tested for electro properties. The resistivity listed above is approximated from experiment data collected both in “Loop” design and “T-shape” design. As shown in Eq.15 and 16, this number has good fits in both experiments, which are mutually supported by each other. However, predicted resistivity of PDMS is lower than the resistivity of liquid-phase PDMS from chemical handbook. Most semiconductors have negative thermal coefficient of electrical resistivity, which means as temperature goes up, electrical resistivity decrease. Due to extremely large electric field across PDMS membrane, it’s reasonable to assume temperature raise during pump activation, which renders cured PDMS membrane become more “permeable” to electric field. However, further analysis should be performed to prove this hypothesis. Optimizations of potential loss fall into two strategies. One is reducing membrane thickness; the other is utilizing conductive PDMS material. The former method is not practical as chances of mechanical failure, like channel collapse or membrane break down, goes up when membrane thickness is reduced. Conductive PDMS is widely used in recent research (31) which provides alternative solution to minimize potential loss across membrane.

The third factor is a combination of screening effect and drag force. We name it underestimation factor as certain flow rates are disregarded in low voltage range. Minimization of drag force is already discussed in early chapter. But currently there is no obvious solution to eliminate screening effect. Corresponding electric field reduction is acceptable with low conductivity buffer, typically in μS/cm scale. With current design, maximum conductivity can go up to 0.5 mS/cm with noticeable fluid motion (experiment data didn't show). However, this number still falls below general value of cell buffer, which limits contactless pump application in cell assay. Possible solution is given by ion permeable silicone hydrogel membrane (32). This kind of membrane removes extra counter ions and prevents ions aggregation. But its fabrication process in microfluidic device is still not applicable for large scale usage.

To summarize, gallium pump has great potential to create relatively large flow rate, 0.3μl/min under current design, which corresponds to 51Pa pumping pressure. With further optimizations, contactless pump is able to provide sufficient pressure difference and mass flow for common biological or chemical usage.

4.4 Implementation in fluid delivery and control system

Fluid delivery and control in LOC products always play one of the essential elements in biological study and analytical chemistry, like purification, chromatography and

screening assay. Typically fluid delivery strategies require external pump or hydrostatic head to provide driven force. Fluid control is usually completed by mechanic valves like Quake valve. These stratifies are well developed and capable to complete laboratory tasks. However, they all suffer from bad portability, reliance on external drive force, and tedious fabrication process somehow. Because gallium pumping unit was isolated from working buffer, it provides simultaneously bidirectional fluid motion control without rearranging electric connections. This advantage gives new clue on fluid delivery and control system design.

Here we propose a new fluid delivery system driven by contact less gallium pump. It is controlled by LabVIEW software. Chip configuration is shown in Fig.8(a) with four pumps aligned at each segment. We want to represent gallium pump has the ability to route fluid into different path, and deliver to certain outlet stream. Fabrication process remained unchanged. Two fluorescent solutions were used to show a direct view of fluid alternation. Solutions filled 4ml wells on external pressure system. Red and Green buffers were directed to inlet1 and inlet2, respectively. 488 and 594 lasers were used again for imaging purpose. By adjusting flow rate in inlet streams, two solution formed clear interface and split evenly into upper stream and right stream. A degasing procedure was followed to eliminate air bubbles. Then we opened three outlets and recovered equal fluid

distribution, shown in Fig.8(a), without pump on. Gallium pump was connected to the DC power distribution system shown in Fig.3 and each pump was controlled through LabVIEW interface. After equilibrium was built, pump1 was activated in a reverse direction, which means pump1 is working against external pressure flow. Applied voltage is pre-calculated based on former characterization to provide sufficient pressure difference to reserve fluid direction. Here we applied 2000V voltage on pump1. Images were captured by DU-8 camera (Nikon).

Due to a relatively large chip dimension, we are not able to image whole chip with current objectives. To acquire a better presentation of fluid motion, we imaged fluid in four corners and reorganized them in Fig.8(b)(c). Buffer1 (red) flows through upper stream(stream4) to outlet1 and left stream(stream3) to outlet2. Similarly, buffer2 (Green) goes through right stream (stream1) to outlet3 and bottom stream (steam2) to outlet2, where two solution form liquid-liquid interface again. When pump1 is on, green solution reverses direction in stream1 and enters stream4. It's corresponding to an interface distortion, shown in Fig.8(c) up-left. It's clear to see when pump1 is acting, control system deliver red buffer to outlet1 instead of outlet1 and outlet2.

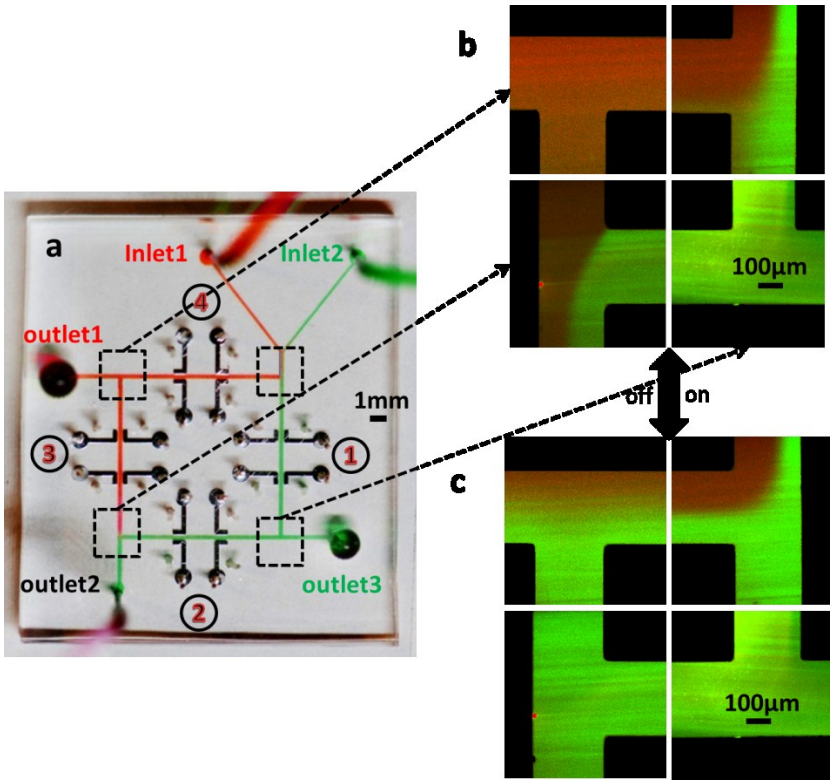

Fig.8 Demonstration of sufficient pumping capacity to alter flow direction and fluid delivery. (a)Two colors split at upper right corner. Red is sent to left and exited at outlet1, then flows down to outlet2. Green goes down to outlet3 and further to outlet2, where two colors recombine together. (b) A combination of four images from each corner, showing fluid distribution under steady state. (c) When pump1 is activated in reverse direction, it creates counter flow against Poiseuille flow. It's large enough to reverse flow direction and pumps green dye upward, results in an interface distortion.

Before we turn on the pump, two solutions split evenly. Red buffer is harvested from upper outlet1 while green is sending to lower right. A combination of two colors comes out of outlet2. After the pump is on, it reverses flow direction in stream1, resulting in

interface shifts to stream4. Mixed solution is collected at upper left while remained outlets only have green dye. Note that there is an obvious diffusion near outlet1 in this experiment which is caused by small flow rate. But it could be minimized by activating multiple pumps at same time through LabVIEW to enhance “routing” ability. This process is facilitated by the manual constructed power distribution system to support each gallium pump independently.

This experiment simulates a fluid delivery and control unit which can be applied to LOC systems, like sequential sample injection, buffer delivery or product collection. Through a programmable control on each pumping unit on chip, flow direction and velocity in each stream become manageable and predictable in LOC products. With pre-calculation, we are able to deliver target stream into specific outlet or reservoir and alter fluid network to discharge waste or washing buffer into different destination. Programmable regulation of pumping process can further accelerate the automation process of this fluid delivery unit and implementation into complex LOC system.

Another advantage shown in this system is the absence of valves. Generally fluid control is achieved by placing valves to block flow channels, which often lead to complicated multi-layer fabrication process and higher possibility of mechanic failures. The system presented here regulated flow pattern with single layer PDMS, which reduced fabrication

consumption and time. One layer fabrication also facilitates large scale manufacturing process like molding and injection. Because of the valveless design, it also served as two directions fluid regulator without blocking fluid path. In other words, with gallium fluid control unit, we can modify a flow rate and achieve continuously fluid motion with much more uniformed fluid velocity. Beyond that, portability is another improvement distinct from traditional control system. Quake valves usually require dead end inlets, which will be filled by water through external water pump, to activate membrane valves. Reliance on external water pump makes it extremely difficult to become a portable system. By eliminating valves, our concept here is to establish a fluid control unit which is independent from external pressure source and complex tubing setup. This concept is proved in plug generation module in next section, which is purely driven by contactless pump. Then fluid delivery and control can be achieved from single DC power source and distribution panel shown in Fig.3. This power system can be further simplified by replacing DC power supply with a high voltage capacitor, which will be discussed in further work. Application of this valveless fluid control system still requires further development as some drawbacks presented in this experiment, like leaky effect, restriction on buffer conductivity and accurate control on blocking fluid. Especially for an unknown system, it is hard to calculate exact voltage requirement to hold buffer in stationary rather than reverse flow direction. However, we believe its advances in

portability and easy-fabrication will still make it a potential trend in LOC fluid deliver and control.

A phenomenon that worth to be noted here is the diffusion effect is very obvious in this fluid network. It may give a clue on utilizing fluid delivery concept in mixing. Mixing is facilities by convection and diffusion. The latter plays a determined role under low Re number system. As shown in Fig.8(c), diffusion effect is already notable at the end of outlet1. If both outlet1 and 3 are closed, by inducing perturbation from each pump, it will hugely increase the contacting area of two solutions and enhance mixing. With proper design, a mix of buffers can circulate inside a closed fluid network until well mixed and collected from a chosen outlet.

4.5 Implementation in sample plug loading device

With the appearance of a new trend in applying microchip capillary electrophoresis (MCE) for analytic chemistry purpose, the limits of current injection technique draw much attention to new module development. Traditional small sample injection strategies are classified at two catalogs, electrokinetic (33) and hydrodynamic (34)(35)(32). Electrokinetic injection is the most common used in MCE due to its independence of external pressure source. It utilizes a cross shape device and EO flow to drive sample solution by applying voltage gradient over inject stream. After sample solution fills the

cross section, potential gradient is switched to flow channel and creates small plug for further analysis. However, this injection strategy, known as electrically floating methods, also leads to sample leaking effect and signal noise in downstream analysis (36). A brief explanation for this leaking effect is provided here. Sample solution inside injecting stream remains stationary when potential gradient is switched, just like "floating" near loading area. When buffer in the other stream starts to move, small amount of sample solution enters flow channel due to the shear force from "EO" flow. This extra sample loading is known as leaking effect, leading to signal noise in optical detection, spectrum or chromatography. On the contrary, hydrodynamic injection provides leak-free sample inducement. But it relies on external pumps to create fluid driven force. It causes to a complex setup of plug generation unit as multiple pressure sources are connected to microfluidic device via tubing. It also limits plug generation rate to the alternation frequency of pressure source. Apparently, hydrodynamic injection has very limited utilizations due to these drawbacks.

Here we present our strategy as a combination of these two principles, which takes advantages of both designs. Gallium pumps aligned with three arms of intersection in cross shape, shown as Fig.9 (a). Both inlets were connected to a small piece of tube filled with fluorescent solutions, serving as fluid reservoir. The left stream was filled with green,

interpreted as sample solution. Red dye, interpreted as buffer solution, filled other three channels. Then we charged pump1 with 2000V to drive buffer down to the channel. At the same time, pump2 was switched on and off periodically through LabVIEW. This impulse loaded sample plug into buffer stream periodically. Then sample plug and buffer solution traveled through detection area downstream. Fluorescent images were acquired by high speed camera (DS-Qi1Mc, Nikon).

Fig.9 (b) is imaged from detection area downstream, under green fluorescent microscope. Sample plug is shown in dark color while buffer solution is in green. Sample plug is formed in a parabolic shape, which proves the driven mechanism is pressure, instead of "EO" flow. Note that plug is not showing a perfect parabola shape, instead, it has longer "tail" on the left. This "tail" shape is caused by bias-injection. Because the driving force is pressure, buffer solution is forced into injecting stream while sending sample downstream. For mass balance, part of sample solution enters buffer stream during this process and forms extra "tail" in sample plug. It only appears on the left side because the other part of injecting stream is filled with buffer instead of sample solution. This is so-called bias-injection. When loading is completed, buffer will repel sample solution back to injecting stream and therefore, eliminating leaking effect.

However, as plug size is no longer confined by cross area dimension, loading volume

requires further calibration by taking extra sample into account. This calibration process will base on former characterization steps to calculate pumped flow mass versus acting time. Pump activation and discharge are fast enough to assume loading process starts instantaneously when pump is charged. So an approximated loading volume will be determined by acting time and charged potential. Another key factor for plug generation unit is producing rate. This rate is directly related to switching frequency, pumping speed, charging and discharging time. With the DC power system, Fig.3, switching frequency is manageable through LabVIEW programing. Charging time for metal electrode or reed relay is relatively fast. So normally pumping speed is the upper limit of generation rate. The higher pumping capability it has, the higher loading frequency we are able to achieve.

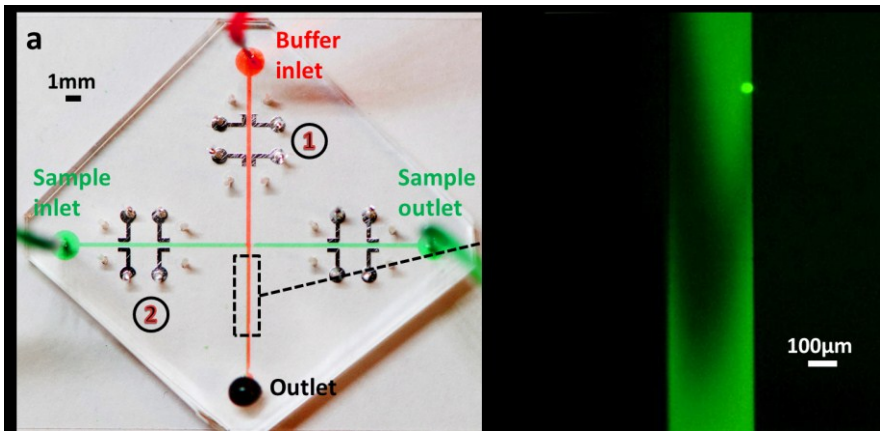

Fig.9 Plug generation unit with gallium pump. (a) An illustration of unit's structure. Tube reservoir provides continues buffer flow driven by pump1. Sample plug is injected into buffer stream and collected at

downstream for further analysis. (b)Image is acquired by green fluorescent microscope.

In this case, we successfully setup a microfluidic pumping system without external pressure support. The whole system is driven by contactless EK pump. The promising aspect of contactless pump in this plug generation system is isolation between electrodes and working fluids. There is no direct contact between sample and electrode, which often leads to denaturation of protein or bio-product due to electrical current or heating. This advantage will expand MCE technology to broader biological applications by minimizing sample damage in analytical process. Besides, working fluid is isolated from EK pumps and electrodes, which means it's possible to establish a closed system for contamination sensitive sample. Contaminations are induced by traditional design from electrode connection area as sample and buffer solutions are exposed to air and electrode material. With contactless system, we can perform pre-sterilization and seal fluid chamber to maintain contamination free environment for biological analysis without exposure from electrodes. On the other hand, we are taking advantage of two injection strategies. By generating plug without external pump and minimized leaking, this unit has great potential by implementation into portable diagnostic device.

Chapter 5 Future work

5.1 Improve efficiency

One of the most obvious limitations of contactless metal pump is the low efficiency. It's the nature of contactless design due to the existence of isolation membrane. Typical materials for isolation membrane are silicon, glass, plastic (polymer), resistivity of these materials are higher than DI water, which leads to increased potential loss as resistivity goes up. Among these materials, PDMS is most common-used polymer for microfluidic molding for its low cost and easy fabrication. But it also has an extremely high resistivity that reduces its applications in micro-electro system.

To improve pumping efficiency and reduce potential loss across PDMS membrane, as we briefly mentioned above, lie in alternations of chip configuration and material properties. As $R = \rho\frac{L}{A}$ Eq.13 described, resistance of PDMS membrane is determined by length and cross section area. By increasing cross section and reducing membrane thickness, we are able to minimize potential loss. However, a reduced membrane thickness also means weak mechanic strength. As PDMS membrane gets thinner, mechanic failures are easier to occur due to a pressure or high voltage. So a balance point must be reached to minimize resistance without sacrifice of system stability. Another direction is optimization of material properties. Conductive PDMS is widely studied in recent years.

Core idea is mixing PDMS with conductive nano-materials, like carbon nanotube (37), or coating PDMS with metallic films (38). However, conductive PDMS recalls some drawbacks from direct contact design, like Joule heating and higher current density. Especially for conductivity lower than DI water, electric circuit may short out flow channel and lead to system design failure. In other words, application of conductive PDMS should be restricted to, and only to isolation membrane, instead of whole chip. It highly depends on fabrication technique advances, like UV curable hydrogel, to fabricate thin membrane between electrode and flow channel.

5.2 Stability Control

We were able to prove that gallium pump provided sufficient flow rate for typical biological or chemical studies. However, many analytical implementations, such as valveless fluid control, loading plug, require precise control on pumping performance. Therefore, deviations of generated pressure or flow rate should be further minimized to an acceptable tolerance.

A main part causing instability is the deviation of PDMS membrane. It was observed that thickness of isolation membrane varied according to gallium injection process. As PDMS is an elastic material, gallium over loading leads to extra pressure inside electrodes. This pressure causes PDMS deformation and thickness variations. The further work of

stability should focus on fabrication process control. Reducing pressure variation and minimize PDMS deformation through standard fabrication process or automotive control is a practical method.

Another out of controlled variation is resistivity of PDMS. From collected data in our work, a uniformed resistivity value from all experiments is around 2e9 Ω·cm, which is much lower than liquid-phase PDMS. We assume this reduction is cause by heating and high voltage treatment. Due to the electric field with magnitude of 10^7 (V/m), PDMS structure may change according to field strength and Joule heating in acting process. It becomes more “porous” or more “permeable” electrical current with unknown reason. Further analysis should focus on material studies, like SEM imaging of low resistivity PDMS membrane, permeability test, and thermal coefficient resistivity test.

5.3 Automation and Scale-up

The final destinations for LOC products may end up in many ways. But portability is always considered due to the nature of LOC and its original concepts. To facilitate further automation and scale up procedure to make real portable analytical platform, we manually assembled the DC power control system with breadboard, reed relays, I/O and PCB board. This system can be used to control individual pump activation through LabVIEW, this includes working time, sequential activation and periodical pumping.

Although this system is independent of external pressure pump, it still involves a bench top high voltage DC power supply to deliver potential difference to gallium pump. Bench top power supply is not suitable for LOC device as portability is limited by its bulky volume. Alternative solution we provide here is DC to HVDC converter called Q-series. The typical volume of Q-series is 0.125 cubic inches, which can be integrated onto breadboard. This converter is able to amplify DC signal from PCB board to up limit of 10000V. With these converters, gallium pump, or other micro-electro system, directly draws power source from laptop and amplifies it to sufficient potential resource. Therefore, the completed microfluidic pumping system is independent of power supply and external pump, purely supported by laptop. This advance will make LOC product a highly portable platform for future commercialization

Chapter 6 Conclusion

We present a new type of metallic based contactless micro-pump is created and characterized in two different experiments. Maximum flow rate and pressure reach 0.3μl/min and 50Pa, respectively. Mathematical prediction of pumping performance is derived from thin double layer EO flow and linear combination of pressure-driven flow. We further modify this model with cofactors for contactless design. Potential optimizations are proposed basing on experiment data analysis. We implement this contactless gallium pump into two microfluidic application modules, fluid delivery and control, plug generation, respectively. Feasibility, troubleshooting and potential optimizations are performed. We expect that, a metallic pump, with low mechanic failure, isolated-working fluid, continues circulating ability and higher portability will facilitate microfluidic device developments in analytic chemistry, screen assay and biological study.

References

1. Huang FC, Liao CS, Lee GB. An integrated microfluidic chip for DNA/RNA amplification, electrophoresis separation and on-line optical detection. Electrophoresis. 2006 08/01;27(16):3297.

2. Gagnon ZR. Cellular dielectrophoresis: Applications to the characterization, manipulation, separation and patterning of cells. Electrophoresis. 2011 09/01;32(18):2466.

3. Buchegger W, Haller A, van dD, Kraft M, Lendl B, Vellekoop M. Studying enzymatic bioreactions in a millisecond microfluidic flow mixer. Biomicrofluidics. 2012 03;6(1):012803.

4. Vladisavljević GT, Khalid N, Neves MA, Kuroiwa T, Nakajima M, Uemura K, et al. Industrial lab-on-a-chip: Design, applications and scale-up for drug discovery and delivery. Adv Drug Deliv Rev. 2013 11/15;65(11–12):1626-63.

5. Harrison DJ, Manz A, Fan Z, Luedi H, Widmer HM. Capillary electrophoresis and sample injection systems integrated on a planar glass chip. Anal Chem. 1992 09/01; 2014/03;64(17):1926-32.

6. Park ES, Difeo MA, Rand JM, Crane MM, Lu H. Sequentially pulsed fluid delivery to establish soluble gradients within a scalable microfluidic chamber array. Biomicrofluidics. 2013 01/09;7(1):11804-.

7. Novo P, Volpetti F, Chu V, Conde JP. Control of sequential fluid delivery in a fully autonomous capillary microfluidic device. Lab Chip. 2013;13(4):641-5.

8. Reichmuth DS, Chirica GS, Kirby BJ. Increasing the performance of high-pressure, high-efficiency electrokinetic micropumps using zwitterionic solute additives. Sensors Actuators B: Chem. 2003 /7/1/;92(1):37-43.

9. Ballerini DR, Li X, Shen W. Flow control concepts for thread-based microfluidic devices. Biomicrofluidics. 2011 03;5(1):014105.

10. D J Laser and JGS. A review of micropumps. J Micromech Microengineering. 2004;14(6):R35.

11. Nguyen N, Huang X, Chuan TK. MEMS-micropumps: A review. Journal of Fluids Engineering. 2002 06/01;124(2):384.

12. van Lintel HTG, van De Pol FCM, Bouwstra S. A piezoelectric micropump based on micromachining of silicon. Sensors and Actuators. 1988 10;15(2):153-67.

13. D J Laser and JGS. A review of micropumps. J Micromech Microengineering. 2004;14(6):R35.

14. Iverson B, Garimella S. Recent advances in microscale pumping technologies: A review and evaluation. Microfluidics and Nanofluidics. 2008 08/01;5(2):145-74.

15. Foroughi P, Zhao Y, Lawler J, Ohadi MM. Development of electrohydrodynamic (EHD) micropumps for cryogenic applications. AIP Conference Proceedings. 2005 02/06;746(1):46-54.

16. Seiler K, Fan ZH, Fluri K, Harrison DJ. Electroosmotic pumping and valveless control of fluid flow within a manifold of capillaries on a glass chip. Anal Chem. 1994 10/01; 2014/04;66(20):3485-91.

17. Eijkel JCT, Dalton C, Hayden CJ, Burt JPH, Manz A. A circular ac magnetohydrodynamic micropump for chromatographic applications. Sensors Actuators B: Chem. 2003 7/1;92(1–2):215-21.

18. Pal S, Datta A, Sen S, Mukhopdhyay A, Bandopadhyay K, Ganguly R. Characterization of a ferrofluid-based thermomagnetic pump for microfluidic applications. J Magn Magn Mater. 2011 11;323(21):2701-9.

19. Moon H, Cho SK, Garrell RL, Kim C"J. Low voltage electrowetting-on-dielectric. J Appl Phys. 2002 10;92(7):4080.

20. Ashraf MW, Tayyaba S, Afzulpurkar N. Micro electromechanical systems (MEMS) based microfluidic devices for biomedical applications. International Journal of Molecular Sciences. 2011 06;12(6):3648-704.

21. Wang P, Chen Z, Chang H. A new electro-osmotic pump based on silica monoliths. Sensors & Actuators B: Chemical. 2006 01/17;113(1):500.

22. Chuan-Hua Chen, Santiago JG. A planar electroosmotic micropump. Microelectromechanical Systems, Journal of. 2002;11(6):672-83.

23. Moncada-Hernandez H, Baylon-Cardiel JL, Pérez-González VH, Lapizco-Encinas BH. Insulator-based dielectrophoresis of microorganisms: Theoretical and experimental results. Electrophoresis. 2011 09/01;32(18):2502.

24. Gencoglu A, Camacho-Alanis F, Nguyen VT, Nakano A, Ros A, Minerick AR. Quantification of pH gradients and implications in insulator-based dielectrophoresis of biomolecules. Electrophoresis. 2011;32(18):2436-47.

25. Hawkins BG, Kirby BJ. Electrothermal flow effects in insulating (electrodeless) dielectrophoresis systems. Electrophoresis. 2010 11/01;31(22):3622.

26. Sridharan S, Zhu J, Hu G, Xuan X. Joule heating effects on electroosmotic flow in insulator-based dielectrophoresis. Electrophoresis. 2011 09/01;32(17):2274.

27. Sano M, Gallo-Villanueva R, Lapizco-Encinas B, Davalos R. Simultaneous electrokinetic flow and dielectrophoretic trapping using perpendicular static and dynamic electric fields. Microfluidics and Nanofluidics. 2013 03/29:1-11.

28. Rice CL, Whitehead R. Electrokinetic flow in a narrow cylindrical capillary. J Phys Chem. 1965 11/01; 2014/03;69(11):4017-24.

29. Reichmuth DS, Chirica GS, Kirby BJ. Increasing the performance of high-pressure, high-efficiency electrokinetic micropumps using zwitterionic solute additives. Sensors Actuators B: Chem. 2003 /7/1/;92(1):37-43.

30. Assael MJ, Armyra IJ, Brillo J, Stankus SV, Wu J, Wakeham WA. Reference data for the density and viscosity of liquid cadmium, cobalt, gallium, indium, mercury, silicon, thallium, and zinc. J Phys Chem Ref Data. 2012 09/00;41(3):033101-16.

31. Li H, Luo CX, Ji H, Ouyang Q, Chen Y. Micro-pressure sensor made of conductive PDMS for microfluidic applications. Microelectronic Engineering. 2010 0;87(5–8):1266-9.

32. Wang J, Liu F. UV-curing of simultaneous interpenetrating network silicone hydrogels with hydrophilic surface. Polymer Bulletin. 2012 09/01;69(6):685-97.

33. Roddy ES, Xu H, Ewing AG. Sample introduction techniques for microfabricated separation devices. Electrophoresis. 2004;25(2):229-42.

34. Lin C, Chen C, Lin C, Chen S. Microchip electrophoresis with hydrodynamic injection and waste-removing function for quantitative analysis. Journal of Chromatography A; 17th International Symposium on Microscale Separations and Capillary Electrophoresis. 2004 /10/8/;1051(1):69-74.

35. - Microchip electrophoresis with hydrodynamic injection and waste-removing function for quantitative analysis. - Journal of Chromatography A. (- 1–2):- 69.

36. Fu L, Lin C. Numerical analysis and experimental estimation of a low-leakage injection technique for capillary electrophoresis. Anal Chem. 2003 11/01; 2014/03;75(21):5790-6.

37. Chen M, Zhang L, Duan S, Jing S, Jiang H, Luo M, et al. Highly conductive and flexible polymer composites with improved mechanical and electromagnetic interference shielding performances. Nanoscale. 2014;6(7):3796-803.

38. Ming-Tsang Lee and Daeho Lee and Alexander Sherry and Costas,P.Grigoropoulos. Rapid selective metal patterning on polydimethylsiloxane (PDMS) fabricated by capillarity-assisted laser direct write. J Micromech Microengineering. 2011;21(9):095018.

Curriculum Vitae

Name: Xiaotong Fu

Address: 3215 North Charles Street, Baltimore, MD, 21218

Email: xfu7@jhu.edu

Phone: 443-326-3622

Education: M.S, Chemical & Biomolecular Engineering, 2014

Johns Hopkins University, Baltimore, MD

B.S, Biotechnology, 2012

Shandong University, China